Hybrid K Based Influential Parameter Determination and Design Optimization of 220 kV High Voltage Insulator

Anik Goswami[1], Paromita Sadhu[2], Pradip Kumar Sadhu[1]

[1]*Department of Electrical Engineering, Indian Institute of Technology, Indian School of Mines, Dhanbad, Jharkhand-826004, India*

[2]*Department of Electrical Engineering, Academy of Technology, Adisaptagram, West Bengal-712121, India*

anik.18dr0026@ee.iitism.ac.in

Abstract—Insulator failure generally occurs due to improper design, and if there exists sharp edges over the insulator surface. There is a need to detect the fragile parameters in the insulator design as they can cause large electrical stress, leading to insulation failure. In this paper, machine learning based approach is used to identify the fragile design parameter and thus determine an optimized design of the insulator, which will eventually decrease the voltage stress over it. A 220 kV insulator is designed and electric field intensity and potential distribution for an assembly of live, ground and insulator is calculated for different geometries. The design parameters of the insulator are considered and varied. The electric field is calculated for the whole assembly of insulator to generate the most optimized design. The optimized design reduces the overall stress by 13.12 %.

Index Terms—Electric Stress; High Voltage; Insulator; Machine Learning Algorithms.

I. INTRODUCTION

Advancement in technology has led to the modernization and urbanization of all the nations across the world. This has increased the need of reliable power supply. One of the major hindrance of which is insulation failure. Insulation failure occurs mainly due to the increase in the electrical stress over the insulator surface. The study of stress on the insulator surface at the solid and air boundary is of prime importance for determining the reliability of the insulator.

In extra high voltage systems, a detailed knowledge of the electric field distribution is necessary for increasing the reliability and life span of the designed insulator. Three-dimensional electrical field calculated from the surface charge simulation method [1], [2] is used in designing optimal insulator. However, in [3] electromagnetic field is obtained using direct boundary element method. The finite element method in [4], [5] shows the electric field and the ion current density generated at the ground level due to the conductors. The insulator contour design is of prime importance as well, in order to have minimal tangential force on the insulator [6]. Genetic algorithm is used for contour optimization of a suspension type insulator with the aim to

minimize the electrical stress [7], [8]. For operation of composite insulators the electric stress on the surface of the insulator is a major factor [9], [10]. In [11], the electrical stress is calculated for 1000 kV insulator using boundary element method and 3-D software package. The shape optimization of the cap and the pin of the insulator is done using Particle Swarm Optimization (PSO). Studies show that the electrical stress depends on the design dimensions of the cap and the pin. Hence, proper design is required to achieve minimum electrical stress on the insulator body [12], [13].

Commercially available insulators fail majorly due to the excessive voltage stress on certain points on the insulator surface. Insulators face high voltage stress generally at bends, sharp edges, and air-dielectric boundaries. There is a need to determine these weak points on the insulator surface, so that adequate precautions can be taken. In this paper, a 220 kV insulator is simulated and the voltage stress over the body of the insulator is studied. The analysis is done by varying the different design parameters of the insulator. Since there is more than one parameter varying, hybrid K algorithm is used to determine the most fragile design parameter [14]. This helps in development of the optimal insulator design. The voltage stress of the designed insulator is reduced significantly, thus reducing the stress at the fragile points. Facilities can monitor the stress at these sensitive points to determine the health of the insulator and take adequate precautions. Manufacturers may use the optimal model to develop insulators with reduced voltage stress, thus improving reliability and improved life expectancy.

II. ELECTRIC FIELD ANALYSIS

Boundary Element Method (BEM) is used for computation of Electric Field. The mathematical foundation of BEM depends on solution of partial differential equations in the region by means of boundary values [15], [16]. It is known as classical boundary value problem. In potential theory the formula is presented as shown in (1)

$$u(x) = \int \delta_{n(y)} \gamma(x,y)[u(y)]\tau d_0(y) -$$
$$-\int_\tau \gamma(x,y)[\delta_{n(y)}u(y)]\tau d_0(y), \qquad (1)$$

for $x \in R^n \setminus \tau$, where $\gamma(x)$ is any fundamental solution of differential equation, $u(x)$ is a harmonic function, δ_n is normal derivative taken with respect to the exterior normal on τ, and d_0 is a surface measure on τ.

For any point i on the electrode surface the potential φ is calculated according to (2)

$$\varphi(i) = \frac{1}{4\pi\varepsilon_0 [\sum_{a=1}^{a'} \int_{S_a} \frac{\sigma(P)}{rP_i} dSa + \sum_{b=1}^{b'} \int_{S_b} \frac{\sigma(Q)}{rQ_i} dSb]}, \quad (2)$$

where s is a surface of the insulator; P is charge density for the region s_a, Q is charge density for the region s_b, r is radius, σ_s is a surface charge density, and ε_0 is the vacuum permittivity.

The potential at any point k due to a surface charge density at any point P located over any surface element s_{se} is given by

$$\varphi_k = \frac{1}{4\pi\varepsilon_0} \sum_{se=1}^{S_E} \int_{S_{se}} \frac{\sigma_{se}}{r_{Pk}} dSe, \quad (3)$$

where s_E is total number of surface elements and

$$\sigma(k) = \frac{2\sigma_s(k)}{\varepsilon_1 + \varepsilon_2} + 2\varepsilon_0 \frac{\varepsilon_1 - \varepsilon_2}{\varepsilon_1 + \varepsilon_2} \times$$
$$\times \sum_{se=1}^{S_E} \int_{S_{se}} \frac{\sigma_{se} \cos(r_{Pk}, n_k)}{r_{Pk}} dse, \quad [P \neq k], \quad (4)$$

where ε_1 is the relative permittivity from side orientation 1, ε_2 is the relative permittivity from side orientation 2.

To obtain the numerical solution of (4), basis function of different order is required for approximating the surface charge σ. The basis function is given by

$$\phi = \sum_{i=1}^{n} N_i \phi_i. \quad (5)$$

The basis function will calculate the value of the function at any given point on that boundary. The basis function is conveniently expressed in L-coordinate system [17]. For triangular boundary the linear approximation is given by

$$\phi = [L_1 L_2 L_3] \begin{vmatrix} \phi_1 \\ \phi_1 \\ \phi3 \end{vmatrix}, \quad (6)$$

where

$$L_1 + L_2 + L_3 = \frac{A_1}{A} + \frac{A_2}{A} + \frac{A_3}{A} = 1, \quad (7)$$

and A is a total area of surface, and A_i is the area between various triangular points.

Boundary elements are approximated by first order polynomial. Hence, for triangular boundary element the number of nodes is 3. The surface charges are located at the vertices of the triangular boundary elements.

The contribution of the observed element to the potential at any arbitrary point G is given by

$$\varphi_{elec} G = \frac{1}{4\pi\varepsilon_0} \times$$
$$\times \int_0^1 \int_0^{1-\varepsilon} \varepsilon\sigma_1 + n\sigma_2 + (\frac{(1-\varepsilon-n)\sigma_3}{r_{IG}(\varepsilon,n)} |J(L_1, L_2)| dL_1 L_2), \quad (8)$$

where $J(L_1, L_2)$ is the Jacobian of the transformation.

If expressed as set of linear equations, then (8) reduces to

$$[A][\sigma] = [V], \quad (9)$$

where $[A]$ is a coefficient matrix, $[V]$ is a column vector describing the potential at the node on the electrode surfaces, and $[\sigma]$ is a matrix of the equivalent charge at the node.

III. HYBRID K BASED CLUSTERING

K-means cluster can create very tight cluster for large number of variables [18]. Whereas linear regression gives very fast results and is used to determine the dependence of one variable on other [19]. The hybrid K clustering algorithm model takes the advantage of both K-means clustering and linear regression. The present problem is a multi-variable optimization problem. The variables do not have a linear relationship among themselves and they are not homogeneous. So, there is a requirement of forming groups among the variables and, then, predicting the output. Thus, traditional regression or K based clustering will not produce good results. Hybrid K based clustering with linear regression model is suitable, in this case, as regression data can become the centroid of the clustered data, which gives better correlation between the variables.

In K-means optimization problem, the loss function is required to be minimized. The loss function is of the form

$$L_k = \sum_{j=1}^{n} \sum_{r \in R} (x_{j,r} - \alpha_{k(j),r})^2, \quad (10)$$

where $\alpha_{k(j)}$ is the centroid of the cluster. The Euclidean distance of a point x_j of a finite set R from the centroid is to be minimized.

In linear regression, the loss function of each point from its regression hyper-plane is given in (11)

$$L_r = \sum_{j=1}^{n} (y_j - (a_{k(j)}^T x_j + b_{k(j)}))^2, \quad (11)$$

where $y = \sum a_k x_j + b_k$ is the linear regression model.

In hybrid K- means optimization, the clustering follows the integrated loss function

$$L_{k,r} = pL_r + (1-p)L_k. \quad (12)$$

In each iteration, the loss function is minimized. When the loss function reaches a global or local optimum, the algorithm stops and, hence, the optimum centroid point is found.

IV. INSULATOR DESIGN

The model under consideration is a 220 kV long rod silicon composite insulator. The description of the model is as follows:
- Number of sheds = 36 (big) + 35 (small) =71;
- Minimum distance between the sheds = 51 mm;
- Creepage distance = 7801 mm;
- Dry arching distance = 1928 mm;
- Angle of the sheds = 6^0.

Figure 1 shows the design specification of the actual insulator.

The parameters under consideration are:
- Flange angle (θ);
- Flange radius (r_0);
- Core radius (r_i);
- Insulator outer edge radius (r_{os});
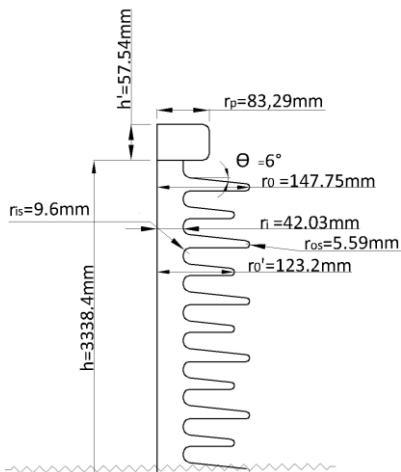- Electrode radius (r_p).

Fig. 1. Insulator design specifications.

The parameter values are varied within the range of practical application and the influence of these variations on the electric field distribution for step voltage is studied.

V. EFFECT OF CHANGE IN FLANGE ANGLE

In this case, the r_0=147.75 mm, r_i=42.03 mm, r_{os}=5.59 mm, insulator height (h) =3338.4 mm, are all kept constant. The slope angle (θ) is originally 6°. Now, it is decreased and increased by 2°, in steps of 1°. The results are presented in Table I. From Table I, it can be observed that for 8° the stress is minimum. So, now the original design is modified and the slope angle is taken as 8°.

TABLE I. CHANGE IN STRESS FOR CHANGE IN SLOPE ANGLE.

Flange angle (θ) in (°)	Electrical Stress (V/m)	Percentage Change (%)
6 (Original)	0.001638	0
5	0.001644	0.366
4	0.001680	2.56
7	0.001634	-0.244
8	0.001602	-2.19

VI. EFFECT OF CHANGE IN FLANGE RADIUS

In this case, the θ=8°, r_i= 42.03 mm, and r_{os}=5.59 mm are all kept constant. The flange radius r_0 and $r_0´$ are decreased and increased by 10 mm.

The variation of the electrical stress with change flange radius is presented in Table II.

TABLE II. CHANGE IN STRESS FOR CHANGE IN FLANGE RADIUS.

Bigger Flange Radius (r_0) (mm)	Smaller Flange Radius ($r_0´$) (mm)	Electrical Stress (V/m)	Percentage Change (%)
147.75	123.2	0.001638	0
127.75	103.2	0.001604	-2.075
137.75	113.2	0.001590	-2.93
157.75	133.2	0.001632	-0.366

From Table II, it is seen that for r_0=137.75 mm and $r_0´$=113.2 mm the stress is minimum. So, now the original design is modified and the slope angle is taken as 8°, and flange radius is taken as r_0=137.75 mm and $r_0´$=113.2 mm.

VII. EFFECT OF CHANGE IN MEAN RADIUS

In this case, the θ=8°, r_{os}=5.59 mm, r_0=137.75 mm, and $r_0´$=113.2 mm, these are all kept constant. The mean radius r_i is decreased and increased by 2 mm. The variation of the electrical stress with the mean radius is presented in Table III.

TABLE III. CHANGE IN STRESS FOR CHANGE IN MEAN RADIUS.

Mean Radius (r_i) (mm)	Electrical Stress (V/m)	Percentage Change (%)
42	0.001638	0
38	0.001648	0.61
40	0.001630	0.488
44	0.001584	-3.29
46	0.001566	-4.39
48	0.001572	-4.02

From Table III, it is seen that for r_i=44 mm the stress is minimum. So, now the original design is modified and the slope angle is taken as 8°, and flange radius is taken as r_0=137.75 mm and $r_0´$=113.2 mm and r_i=44 mm.

VIII. EFFECT OF CHANGE IN OUTER RADIUS

In this case, the θ=8°, r_0=137.75 mm, $r_0´$=113.2 mm, and r_i=44 mm, these are all kept constant. The outer radius r_{os} is decreased and increased by 1 mm. The variation of the electrical stress with the outer radius is presented in Table IV.

TABLE IV. CHANGE IN STRESS FOR CHANGE IN OUTER RADIUS.

Outer Radius (r_{os}) (mm)	Electrical Stress (V/m)	Percentage Change (%)
5.59	0.001638	0
4.59	0.00164	0.12
3.59	0.001647	0.55
6.59	0.001475	-9.95
7.59	0.001705	4.09

From Table IV, it is seen that for r_{os}=6.59 mm the stress is minimum. With a decrement of 1 mm from the original outer radius the electric stress on the insulator is decreased by 9.95 %. So, now the original design is modified and the slope angle is taken as 8°, and flange radius is taken as

r_0=137.75 mm, and r_0'=113.2 mm, and r_i=44 mm, and r_{os}=6.59 mm. The next change is to vary the electrode radius.

IX. EFFECT OF CHANGE IN ELECTRODE RADIUS

In this case, the θ=8°, r_{os}=6.59 mm, r_0=137.75 mm, r_0'=113.2 mm, and r_i=44 mm, these are all kept constant. The electrode radius r_p is decreased and increased by 5 mm. The variation of the electrical stress with change electrode radius is presented in Table V.

TABLE V. CHANGE IN STRESS FOR CHANGE IN ELECTRODE RADIUS.

Electrode Radius (r_p) (mm)	Electrical Stress (V/m)	Percentage Change (%)
83.29	0.001638	0
73.29	0.001523	-7.02
78.29	0.001500	-8.42
88.29	0.001450	-11.47
92.29	0.001423	-13.12

From Table V, it is seen that for r_p=92.29 mm the stress is minimum. So, now the original design is modified and the slope angle is taken as 8°, flange radius is taken as r_0=137.75 mm, and r_0'=113.2 mm, and r_i=44 mm, and r_{os}=6.59 mm, and r_p= 92.29 mm.

X. PREDICTION OF INFLUENTIAL DESIGN PARAMETER

An analysis is carried to find out the dependence of the output on the input parameters and, hence, determine the most critical input parameter. Table VI shows the analysis of variance.

TABLE VI. ANALYSIS OF VARIANCE.

Source	DF	Sum of Squares	Mean Square	F Value	Pr > F
Model	1	4.30268 ×10-8	4.302686 ×10-8	10.72	0.0040
Error	19	7.62382 ×10-8	4.012254 ×10-9	--	--
Corrected Total	20	1.92651 ×10-7	-2.93 %	--	--

The gradient of the predictor variable is 0, as seen from the F value test. The p-value being small (less than 0.05), there is adequate indication to reject the null hypothesis at the 0.5 significance level. It is seen that the hybrid linear regression model suits the data better than the baseline model [20].

TABLE VII. SUMMARY OF THE MEASURES.

Root MSE	R- Square	Dependent Mean	Adj R-Square	Coeff Var
0.0000633	0.3608	0.00159	0.3271	3.977

From Table VII, it is observed that the proportion of variability witnessed in the data is 0.3608. So, 36 % of the total deviation in the output values can be explained by the regression line.

XI. MODEL BUILDING AND INTERPRETATION

The objective is to determine the Linear Regression task for model selection. Each of design parameters are assigned

with a variable:
- X_1 = Flange angle (θ);
- X_2 = Flange radius (r_0);
- X_3 = Core radius (r_i);
- X_4 = Insulator outer edge radius (r_{os});
- X_5 = Electrode radius (r_p).

Table VIII shows the result of linear regression. Mallow's C_p and Hocking's Criteria are used to indicate model bias [21]. The models having C_p values near to p (the number of variables in the design and the intercept) are considered.

TABLE VIII. LINEAR REGRESSION RESULTS.

| Model Index	Number in Model	C_p	R-Square	Variables in Model
1	2	5.0321	0.4838	X3 X4
2	3	5.0936	0.5338	X2 X3 X4
3	3	5.1076	0.5334	X1 X3 X4
4	3	5.1742	0.5317	X3 X4 X5
5	4	5.2278	0.5818	X2 X3 X4 X5
6	4	5.2430	0.5814	X1 X3 X4 X5
7	2	5.8420	0.4629	X2 X4
8	4	5.8698	0.5653	X1 X2 X3 X4
9	3	5.8717	0.5137	X1 X2 X4
10	5	6.0000	0.6135	X1 X2 X3 X4 X5
11	3	6.0234	0.5098	X2 X4 X5
12	4	6.1405	0.5609	X1 X2 X4 X5
13	2	6.1579	0.4548	X1 X4
14	3	6.3446	0.5015	X1 X4 X5
15	1	7.8072	0.3608	X4
16	2	8.0182	0.4069	X4 X5
17	2	12.178	0.2997	X2 X3
18	2	12.255	0.2977	X1 X3
19	3	12.403	0.3454	X2 X3 X5
20	3	12.482	0.3434	X1 X3 X5
21	1	12.511	0.2396	X3
22	2	12.746	0.2850	X3 X5
23	3	12.758	0.3362	X1 X2 X3
24	4	12.978	0.3821	X1 X2 X3 X5
25	2	15.176	0.2224	X1 X2
26	3	15.466	0.2665	X1 X2 X5
27	1	15.904	0.1521	X2
28	2	16.213	0.1957	X2 X5
29	1	16.564	0.1351	X1
30	2	16.882	0.1785	X1 X5
31	1	20.162	0.0424	X5
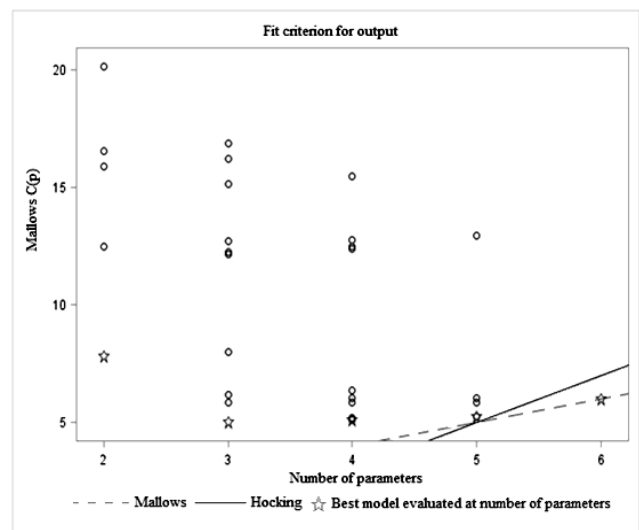
Fig. 2. Mallow's C(p) plot.

The model with the fewest variable, where C_p value is taken close to p, (13) gives the estimate of C_p

$$C_p = m + \frac{(MSE_m - MSE_{tot})(n-m)}{MSE_{tot}}, \qquad (13)$$

where MSE_m is the mean squared error for the model with m parameters, MSE_{tot} is the mean squared error of the complete model used to determine the actual residual value, n is the number of observation, and m is the number of parameters including the intercept parameter.

From Fig. 2, it is observed that the best model is evaluated when the number of parameters is 4.

XII. INFLUENTIAL PARAMETER ANALYSIS

Influential parameter is determined using Cook's D analysis [22]. As it can be seen in Fig. 3, the observation 14 is maximum and the value is 1.85, which is much more than three times the mean value, which is 0.25. So, according to the thumb rule, it can be concluded that observation 14 in Table VIII is the possible outliner.
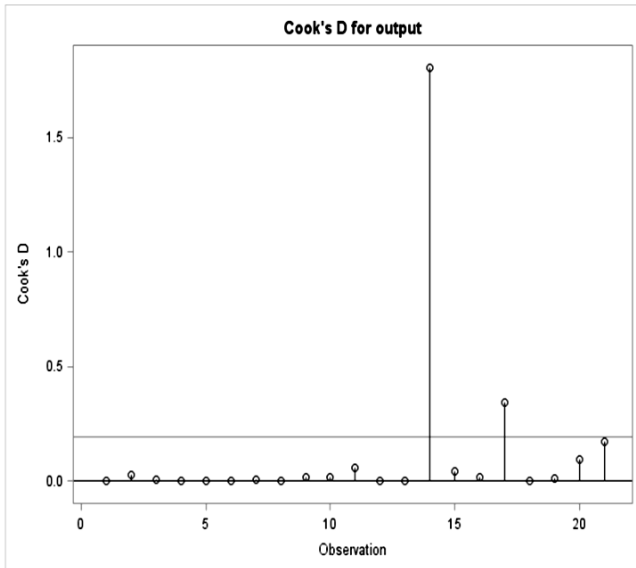

Fig. 3. Cook's D plot for the model.

Figure 4 gives the DFFITS plot [23]. From Fig. 4, it is observed that X_4 has the highest influence on the output of the model. X_4 is having a value of 4, which is much higher than the values of the other inputs.
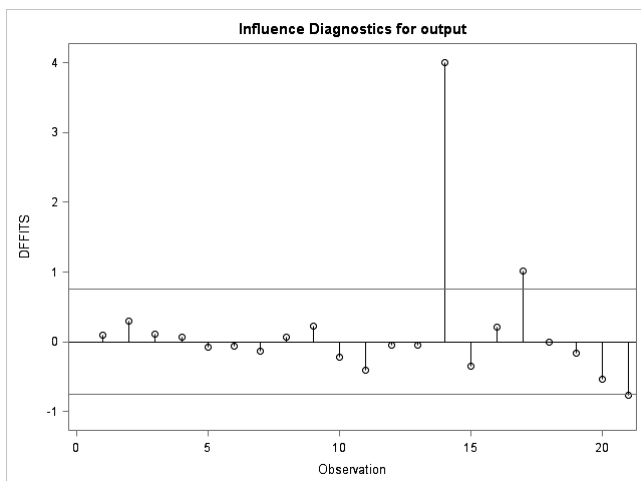

Fig. 4. DFFITS plot for the model.

From DFBETAS plot in Fig. 5, it is observed that X_4 has the highest influence on the output. From the three influence models, it can be concluded that the parameter X_4 (insulator outer edge radius) is the most important parameter in the design of the insulator.
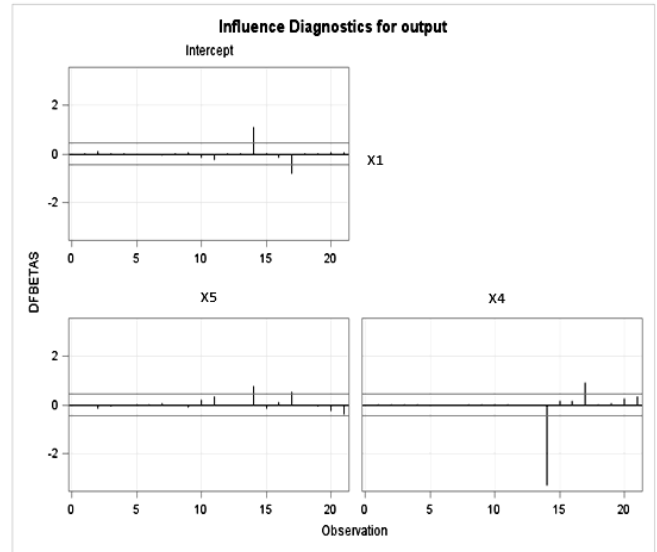

Fig. 5. DFBETAS plot for the model.

XIII. RESULTS AND DISCUSSIONS

From Table I,II,III,IV, and V, it can be observed that the design configuration that leads to the minimum electrical stress on the insulator is when slope angle is taken as $8°$ and flange radius is taken as $r_0= 137.75$ mm, and $r_0{'}=113.2$ mm, and $r_i=44$ mm, and $r_{os}=6.59$ mm, and $r_p=92.29$ mm. A data set of 15000 input parameters is taken as the training set for the simulation using hybrid K based clustering approach. Another data set, consisting of 3000 data, is taken as testing input. Each epoch consisted of 36 samples out of the 15000 input parameters, the iteration was continued till the whole set is traversed. Form Table VI, it is seen that the mean square error is 4.012254×10^{-9} and having a corrected total of 1.92651×10^{-7}. The corrected total signifies that the difference between the training set and the testing set is very low and the output is having a high accuracy. This suggests that the trained network performed an excellent job in predicting the electrical stress at each point. From Table VII, it is seen that the regression line explains 36 % of the total variation in the response values From Mallow's C_p test and Hocking's criteria, it is predicted that the output presents the highest accuracy when the number variable of input parameters is taken as 4. From Cook's plot, it is observed that flange angle (θ), insulator outer edge radius (r_{os}), and electrode radius (r_p) are the most influential parameters, which have a huge impact on the electric stress distribution on the insulator. To find out a single design parameter having the highest impact on electrical stress distribution, DFFITS and DFBETAS plots are used. These plots signify that input parameter X_4 or insulator outer edge radius (r_{os}) are the most influential parameters in insulator sizing. Maximum stress occurs on the insulator outer edge radius and chances of insulation breakdown is high in this area. To improve the reliability of the high voltage insulator, the outer edge radius must be designed carefully, so that it can withstand the high electrical stress occurring on it.

XIV. CONCLUSIONS

A 220 kV suspension type long rod silicon based insulator having 71 sheds is designed. To reduce the electrical stress on the insulator, design optimization is done and the effect on the electrical stress is studied. The design parameters includes flange angle, flange radius, core radius, insulator outer edge radius, and electrode radius. One parameter is changed at a time while keeping others constant and the electrical stress is calculated. The design, which gives the minimum electrical stress, is taken and, then, the other parameters are varied. In this way, for each parameter the design, which gives the minimum stress, is taken and, finally, the optimized design is obtained. Further it was required to determine the dependence of the output on the input design parameters, so that it helps in finding the fragile design parameter. It is observed that the parameter insulator outer edge radius is the most influential in affecting the electrical stress on the insulator. The design, presented in this paper, helps in reducing the electrical stress by 13.2 % and determining the most influential design parameter. This will facilitate better health monitoring, improved life, and reliability of the insulator.

REFERENCES

[1] M. Talaat, A. El-Zein, and M. Amin, "Electric field simulation for uniform and FGM cone type spacer with adhering spherical conducting particle in GIS", *IEEE Transactions on Dielectrics and Electrical Insulation*, vol. 25, no. 1, pp. 339–351, 2018. DOI: 10.1109/TDEI.2018.006980.

[2] Y. Lv, J. Li, X. Zhang, G. Pang, and Q. Liu, "Simulation study on pollution accumulation characteristics of XP13-160 porcelain suspension disc insulators", *IEEE Transactions on Dielectrics and Electrical Insulation*, vol. 23, no. 4, pp. 2196–2206, 2016. DOI: 10.1109/TDEI.2016.7556495.

[3] M. Costabel, and F. J. Sayas, "Time-dependent problems with the boundary integral equation method", in *Encyclopedia of Computational Mechanics Second Edition*, pp. 1–24, 2017. DOI: 10.1002/9781119176817.ecm2022.

[4] J. Jiao, L. Li, B. Wu, and C. He, "Novel capacitive proximity sensors for assessing the aging of composite insulators", *Sensors and Actuators A: Physical*, vol. 253, pp. 75–84, 2017. DOI: 10.1016/j.sna.2016.11.025.

[5] S. M. Ale-Emran and M. Farzaneh. "Parametric studies and improved hypothesis of booster-shed effects on post insulators under heavy icing conditions", *IEEE Transactions on Dielectrics and Electrical Insulation*, vol. 22, no. 1, pp. 420–427, 2015. DOI: 10.1109/TDEI.2014.004619.

[6] M. Bouhaouche, A. Mekhaldi, and M. Teguar, "Improvement of electric field distribution by integrating composite insulators in a 400 kV AC double circuit line in Algeria", *IEEE Transactions on Dielectrics and Electrical Insulation*, vol. 24, no. 6, pp. 3549–3558, 2017. DOI: 10.1109/TDEI.2017.006011.

[7] S. A. Bessedik, R. Djekidel, and A. Ameur, "Performance of different kernel functions for LS-SVM-GWO to estimate flashover voltage of polluted insulators", *IET Science, Measurement & Technology*, vol. 12, no. 6, pp. 739–745, 2018. DOI: 10.1049/iet-smt.2017.0486.

[8] S. Zhao, X. Jiang, and Y. Xie, "Evaluating the contamination level of polluted insulators based on the characteristics of leakage current", *International Transactions on Electrical Energy Systems*, vol. 25, no. 10, pp. 2109-2123, 2015. DOI: 10.1002/etep.1951

[9] K. H. Lee, S. G. Hong, M. K. Baek, H. S. Choi, Y. S. Kim, and I. H. Park, "Alleviation of Electric Field Intensity in High-Voltage System by Topology and Shape Optimization of Dielectric Material Using Continuum Design Sensitivity and Level Set Method", *IEEE Transactions on Magnetics*, vol. 51, no. 3, pp. 1–4, 2015. DOI: 10.1109/TMAG.2014.2358845.

[10] J. A. Virbalis, R. Lukocius, P. Marciulionis, G. Nedzinskaite, and P. Vaskys, "Investigation of the electric field of metallic fence under a high voltage transmission line", *Elektronika ir Elektrotechnika*, vol. 22, no. 6, pp. 22–27, 2016. DOI: 10.5755/j01.eie.22.6.17218.

[11] J. Wang, B. Vue, X. Deng, T. Liu, and Z. Peng, "Electric field evaluation and optimization of shielding electrodes for high voltage apparatus in ±1100 kV indoor DC yard", *IEEE Transactions on Dielectrics and Electrical Insulation*, vol. 25, no. 1, pp. 321–329, 2018. DOI: 10.1109/TDEI.2018.006890.

[12] D. Rabah, C. Abdelghani, and H. Abdelchafik, "Efficiency of some optimisation approaches with the charge simulation method for calculating the electric field under extra high voltage power lines", *IET Generation, Transmission & Distribution*, vol. 11, no. 17, pp. 4167–4174, 2017. DOI: 10.1049/iet-gtd.2016.1297.

[13] M. Sarajlic, P. Kitak, and P. Pihler, "New design of a medium voltage indoor post insulator", *IEEE Transactions on Dielectrics and Electrical Insulation*, vol. 24, no. 2, pp. 1162–1168, 2017. DOI: 10.1109/TDEI.2017.005947.

[14] R. Stanforth, E. Kolossov, and B. Mirkin, "Hybrid k-Means: Combining Regression-Wise and Centroid-Based Criteria for QSAR" in *Selected Contributions in Data Analysis and Classification*, Berlin Heidelberg: Data Analysis, and Knowledge Organization. Springer, pp. 225–233, 2007. DOI: 10.1007/978-3-540-73560-1_21.

[15] M. Costabel, "Principles of Boundary Element Methods", *Computer Physics Reports*, vol. 6, pp. 243–274, 1987. DOI: 10.1016/0167-7977(87)90014-1.

[16] T. H. Fawzi and Y. Safar, "Boundary methods for the analysis and design of high voltage insulators", *Computer Methods in Applied Mechanics and Engineering*, vol. 60, pp. 343–369, 1987. DOI: 10.1016/0045-7825(87)90139-3.

[17] P.B. Zhou, *Numerical Analysis of Electromagnetic Fields*. Germany, Berlin: Springer-Verlag, 1993. DOI: 10.1007/978-3-642-50319-1.

[18] M. D. Cattaneo, M. Jansson, and W. K. Newey, "Inference in linear regression models with many covariates and heteroscedasticity", Journal *of the American Statistical Association*, vol. 113, no. 523, pp. 1350–1361, 2018. DOI:10.1080/01621459.2017.1328360.

[19] D. Cheng, Y. Shi, T. Lin, B. H. Gwee, and K. A. Toh, "Hybrid K Means Clustering and Support Vector Machine Method for via and Metal Line Detections in Delayered IC Images", *IEEE Transactions on Circuits and Systems II: Express Briefs*, vol. 65, no. 12, pp. 1849–1853, 2018. DOI: 10.1109/TCSII.2018.2827044.

[20] H. Harb, A. Makhoul, and R. Couturier, "An Enhanced K-Means and ANOVA-Based Clustering Approach for Similarity Aggregation in Underwater Wireless Sensor Networks", *IEEE Sensors Journal*, vol. 15, no. 10, pp. 5483–5493, 2015. DOI: 10.1109/JSEN.2015.2443380.

[21] D. Derryberry, K. Aho, J. Edwards, and T. Peterson, "Model selection and regression t-statistics", *The American Statistician*, vol. 72, no. 4, pp. 379–381, 2018. DOI: 10.1080/00031305.2018.1459316.

[22] J. Koskinen, P. Wang, G. Robins, and P. Pattison, "Outliers and Influential Observations in Exponential Random Graph Models", *Psychometrika*, vol. 83, no. 4, pp. 809–830, 2018. DOI: 10.1007/s11336-018-9635-8.

[23] T. S. Açar, and M. R. Özkale, "Influence measures based on confidence ellipsoids in general linear regression model with correlated regressors", *Journal of Applied Statistics*, vol. 43, no. 15, pp. 2791–2812, 2016. DOI: 10.1080/02664763.2016.1144726.